IET Microwaves, Antennas & Propagation

*Research Article*

IET Journals
The Institution of Engineering and Technology

# Wideband multiple-input–multiple-output dielectric resonator antenna

ISSN 1751-8725
Received on 23rd June 2016
Revised 7th September 2016
Accepted on 11th October 2016
E-First on 16th February 2017
doi: 10.1049/iet-map.2016.0515
www.ietdl.org

*Abhishek Sharma*[1] ✉, *Animesh Biswas*[1]

[1]*Department of Electrical Engineering, IIT Kanpur, Kanpur-208016, Uttar Pradesh, India*

✉ *E-mail: abhisheksharma.rf@gmail.com*

**Abstract:** A two-element multiple-input–multiple-output (MIMO) dielectric resonator antenna having wideband characteristics is presented. The wideband operation is achieved by using a mushroom shaped dielectric resonator excited by a conformal trapezoidal patch. In order to realise two-element MIMO configuration, two wideband radiators are arranged orthogonally which offers polarisation diversity. The measured bandwidth (VSWR ≤ 2) for *Port1* is 61% (5.08–9.50 GHz), whereas for *Port2* it is 65% (4.89–9.61 GHz). The isolation between the two ports is better than 20 dB for the desired frequency band. The antenna exhibits broadside radiation with cross polar level below 15 dB. The peak gain of antenna varies from 3.34 to 7.40 dBi at *Port1* and from 2.34 to 7.9 dBi at *Port2*. Moreover, the various MIMO performance metrics including envelope correlation coefficient (ECC), diversity gain, channel capacity loss and total active reflection coefficient are investigated. The ECC is less than 0.01 and capacity loss is under 0.5 bps/Hz throughout the operating bandwidth. The results confirm that the antenna offers effective MIMO/diversity performance. The proposed antenna can be suitable for WLAN and upper ultra wideband frequency band applications.

## 1 Introduction

Claude Shannon's information theory [1] suggested that there exist an upper limit for the channel capacity using a single transmitter and single receiver. In the late 1990s, extensions to Shannon's capacity limit has been independently proposed by Telatar and Foschini for wireless system using multiple antenna elements at transmitter and receiver end [2]. The use of multiple antennas on transmit/receive ends surpasses the previous limit proposed by Shannon for the single antenna. This spurred huge interest among antenna engineers to design multiple-input–multiple-output (MIMO) antennas which now became the most appropriate candidate for modern day high speed wireless communication systems. MIMO technology provides improved channel capacity, higher data rate, link reliability in multipath channels [3–5].

Over the last few years, a considerable amount of work has been done in planar and metallic-based MIMO antennas [6–13]. For instance in [6], a MIMO array antenna comprising printed inverted F-antenna embedded with U-shaped slot has been presented for wireless broadband applications. A dual-broadband MIMO antenna system comprising of two opened loops has been investigated for GSM/UMTS/long term evolution (LTE) and WLAN handsets [7]. A wideband printed MIMO monopole antenna consisting of crescent shaped radiators has been reported for WiFi/WiMAX applications [8]. In [9], a printed two monopole antenna system along with neutralisation line as a decoupling network has been proposed for wireless USB-dongle applications. In [10–12], MIMO antennas for ultra wideband (UWB) applications have been investigated. A four-element quad-band MIMO antenna where a CPW-fed monopole loaded with split-ring resonator and interdigital capacitor has been reported for GSM/Bluetooth/WLAN/WiMAX applications [13]. A compact broadband dual-polarised antenna has been proposed for indoor MIMO wireless communication system in [14].

The main drawback with the metallic antennas is that at high frequency the conductor loss become severe and antenna efficiency drops significantly. On the other hand, the dielectric resonator antennas (DRAs) have proven to be the best alternative of metallic antennas because of numerous advantages such as light weight, small size, no inherent conductor loss, relatively wide bandwidth, high efficiency etc. [15]. However, a very few DRA based MIMO antennas were available in open literature [16–26]. The concept of DRA based MIMO antenna was first described by Ishimiya *et. al.* [16, 17], where around 10 dB diversity gain has been achieved with the performance comparable with traditional MIMO antennas. A MIMO DRA for LTE femtocell base stations is presented in [18] where for MIMO operation, the mode degeneracy was induced using boundary perturbation such that TE and HE modes of the DRA will resonate at the same frequency. In [19], a $2 \times 2$ MIMO system has been realised and propagation channel characteristics has been investigated based on complex scattering parameters (S-Parameters) between the transmitting and receiving MIMO antennas. A frequency agile half split MIMO cylindrical DRA has been experimentally demonstrated in [20] for femtocell base-stations applications. In [21], a MIMO rectangular DRA at 2.6 GHz for 4G LTE application has been proposed, where two of the orthogonal modes were excited using CPW inductive slot and coaxial probe. An eight-port compact cylindrical DRA with different polarisation states (LHCP, RHCP, and LP) has been designed for MIMO communication system [22]. An eight-element low profile, dual-band MIMO DRA for wireless access points has been presented in [23]. In [24, 25], the authors have proposed a millimetre-wave MIMO DRA array operating at 30 GHz for hand-held devices. In [26, 27], the authors have reported DRA based MIMO antenna for 4G applications.

In this paper, a dual element wideband MIMO DRA offering polarisation diversity is presented. The wide bandwidth is realised using mushroom shaped DR excited by a conformal trapezoidal patch. In order to study the MIMO/diversity performance various metrics such as envelope correlation coefficient (ECC), diversity gain, channel capacity loss (CCL) and total active reflection coefficient (TARC) are evaluated. All the simulations are done in Ansoft HFSS and a prototype of same is built and tested.

## 2 Wideband mushroom shaped DRAs design

Before embarking on the details of wideband MIMO DRA, initially a mushroom-shaped DRA is designed possessing wideband characteristic.

The mushroom shaped DR can be seen in two parts, where the lower part is a square DR of length $L$ and height $H$ and the upper DR is a half split cylindrical DR of radius $R$ with both the DRs

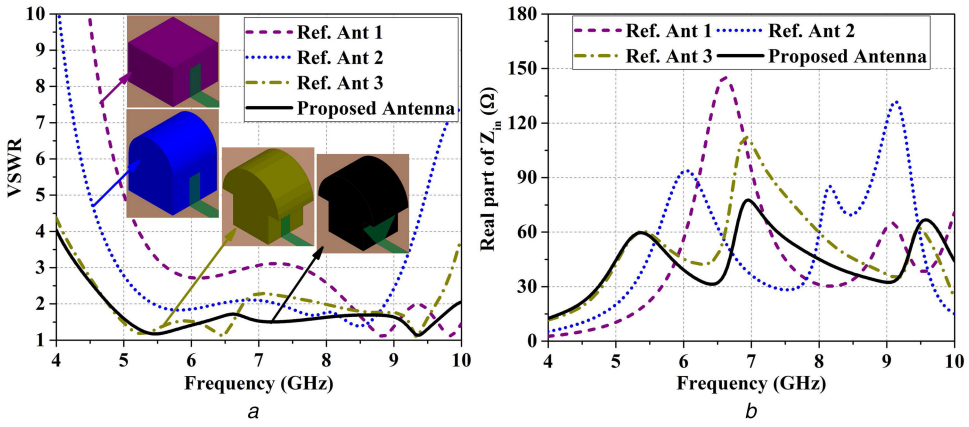


**Fig. 1** *Response of reference antennas and proposed antenna*
***(a)*** Simulated VSWR, ***(b)*** Simulated real part of input impedance

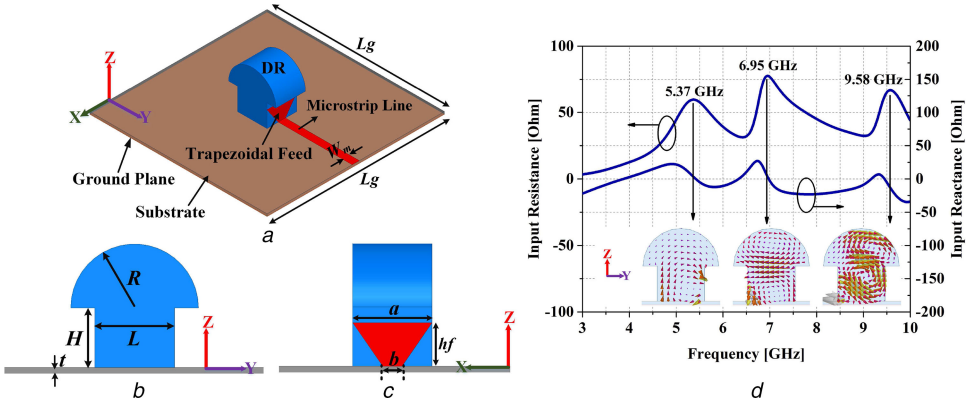


**Fig. 2** *Geometry of proposed antenna ($L_g$ = 60 mm, R = 8 mm, L = 10 mm, H = 7.5 mm, $W_m$ = 2.4 mm, t = 0.787 mm, a = 10 mm, b = 2.4 mm)*
***(a)*** Isometric view, ***(b)*** Front view, ***(c)*** Left view, ***(d)*** Simulated input impedance response of wideband mushroom shaped DRA

having same dielectric constant ($\epsilon_r = 10.2$). The antenna is designed in four stages as shown in inset of Fig. 1*a*. First, a square DR of length $L$ and height $H$ is excited by conformal rectangular strip (CRS) which generates multiple resonances (indicated by the peak of real part of input impedance (Fig. 1*b*) and is referred as Ref. Ant 1. Second, the Ref. Ant 2 (dome shaped) is constructed by putting a half split cylindrical DR for radius $R = L/2$ over the square DR and is excited through the same CRS. Next, the Ref. Ant 2 is transformed into mushroom shaped DR having the optimised radius of $R = 0.8L$ and is termed as Ref. Ant 3. It is observed that, the higher side of frequency band is not matched in case of Ref. Ant 3 and hence it does not provide VSWR ≤ 2 in the desired frequency band. Finally, the feeding strip is optimised to ensure a good matching throughout the desired frequency band.

The geometry of the proposed antenna is shown in Fig. 2. The mushroom shaped DR is place at the centre of a low permittivity ($\epsilon_{rs} = 2.2$) substrate of dimension 60 mm × 60 mm × 0.787 mm. The antenna is excited by a conformal patch [28–30] which is attached to the side wall of DR and is connected to 50 Ω microstrip line. The feed has top width $a$, bottom width $b$, and height $hf$ as shown in Fig. 2*c*. The conformal strip/patch excitation is an effective feeding mechanism, where it is easier to couple the energy between feed and DR, which helps in the matching and excitation of different modes that merges together to provide wider bandwidth.

The mushroom shaped DR is resonating at three different frequency (5.37, 6.95, and 9.58 GHz) as depicted in Fig. 2*d* with respective resistances of around 60, 77 and 66 Ω, respectively. Inset of Fig. 2*d* shows the simulated E-field distribution at three different frequencies (5.37, 6.95, and 9.58 GHz), where the three modes namely $TE_{111}$, $TE_{113}$, $TE_{115}$ are observed. It is also observed that the electric field loops of higher order $TE_{115}$ mode are tilted few degrees with respect to the $z$-axis. This mode can be considered as a deformed version of $TE_{115}$ mode which might affect the radiation pattern and cross polarised levels at higher frequency.

The feed dimensions mainly the feed height $hf$ and feed top width $a$, controls the coupling between the trapezoidal patch and DR. Hence, a parametric analysis is carried out to investigate the effect of feed dimensions. Fig. 3*a* shows the simulated VSWR for different values of feed height $hf$ and a pronounce effect of $hf$ is revealed.

It is found that the better matching occurs in the desired frequency band when the feed height is 5.5 mm. The simulated VSWR for different values of feed top width $a$ keeping other parameters constant is presented in Fig. 3*b*. It is observed that the bandwidth increases as $a$ increases from 2 to 10 mm. Beyond $a$ = 10 mm, the feed top width exceeds the base dimension $L$ of the DRA and hence, for the final design $a$ = 10 mm is considered for the maximum bandwidth. The dimension of the bottom width $b$ (= 2.4 mm) is chosen same as the width of 50 Ω microstrip line. From the above parametric study, the optimised feed dimensions are found to be $a$ = 10 mm, $b$ = 2.4 mm and $hf$ = 5.5 mm.

To validate the design, a prototype is built using RT/Duroid 6010 of relative permittivity $\epsilon_{rd} = 10.2$ and $\tan\delta = 0.002$. For constructing the trapezoidal patch feed, a copper tape of thickness 80 $\mu$m is used which adhere to the surface of DRA using commercially available adhesive. Fig. 4 shows the comparison between simulated and measured VSWR of the proposed antenna. The simulated and measured bandwidth (for VSWR ≤ 2) is 71% (4.77–9.95 GHz) and 74.4% (4.56–9.96 GHz), respectively.

The deviation in simulated and measured results may be attributed to the air gap that exists between the low permittivity substrate and DR and a slight misalignment of DR. Although, a very thin layer of adhesive is used for bonding but still it might affect the measurement as well. The proposed antenna is radiating (radiation pattern is not shown for brevity) in broadside direction.

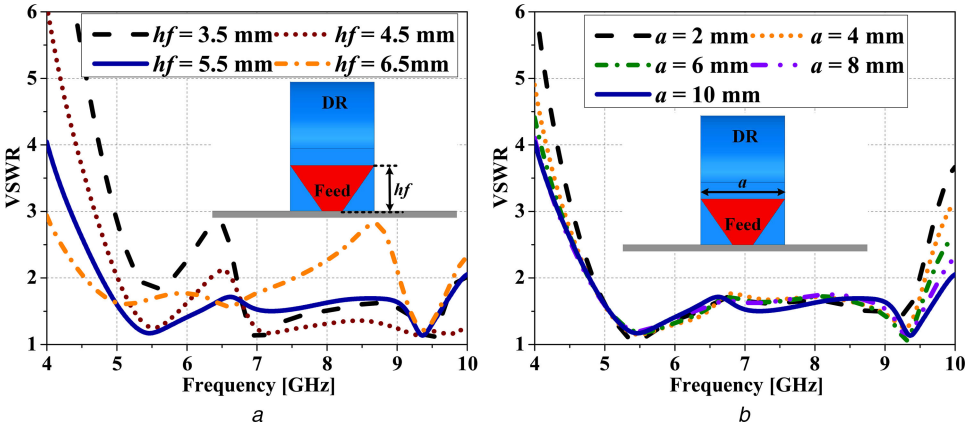


**Fig. 3** *Effect of varying feed dimensions of the wideband mushroom shaped DRA*
***(a)*** Variation of VSWR with hf, ***(b)*** Variation of VSWR with a

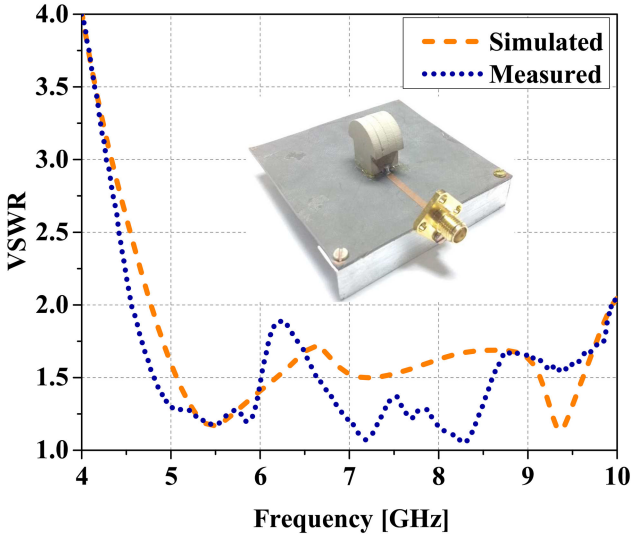


**Fig. 4** *Simulated and measured VSWR of the wideband mushroom shaped DRA*

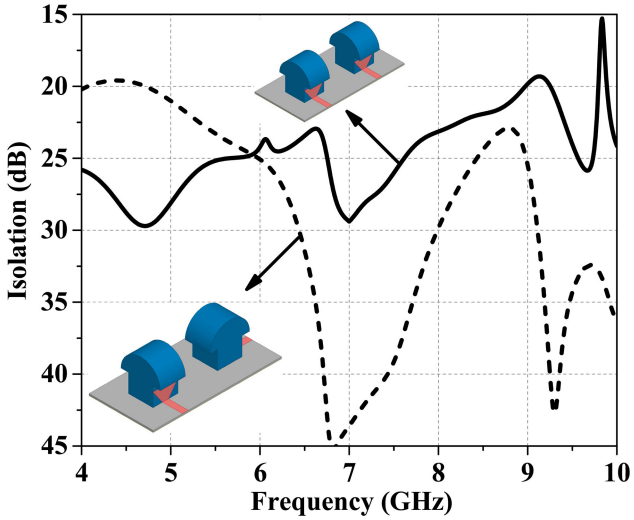


**Fig. 5** *Isolation performance comparison between parallel configuration and orthogonal configuration of MIMO DRA*

## 3 Dual element wideband MIMO DRA

The antenna designed in preceding section is now exploited to realise dual element wideband MIMO DRA.

First, the isolation performance of the parallel and orthogonal configuration of MIMO DRA is compared as shown in Fig. 5. The result shows that the isolation of the orthogonal configuration is better than the parallel configuration. Moreover, to achieve the polarisation diversity and to have a good MIMO performance with low correlation, the orthogonal configuration is studied further. A schematic of the proposed dual element MIMO DRA is depicted in Fig. 6*a*. The inter element spacing *s* governs the mutual coupling between the adjacent antenna elements. Fig. 6*b* depicts the effect of inter element distance *s* on the isolation performance of the proposed MIMO DRA. It is observed that on increasing *s* the isolation increases. For the proposed antenna, the value of *s* is chosen as 13 mm, to ensure more than 20 dB isolation throughout the bandwidth along with compact size.

Fig. 7*a* shows the simulated and measured VSWR response of the proposed MIMO DRA. The simulated and measured bandwidth (for VSWR $\leq 2$) for *Port1* is 63% (4.97–9.85 GHz) and 61% (5.08–9.5 GHz), respectively and for *Port2*, the same is 64% (5.12–10 GHz) and 65% (4.89–9.61 GHz), respectively.

From Fig. 7*b*, it is observed that both the simulated and measured isolation between the two ports is better than 20 dB over the entire spectrum.

Normalised radiation pattern of the antenna element 'DRA-1' in *xz*- and *yz*-plane with port 2 terminated with matched load is shown in Fig. 8. The proposed antenna exhibits broadside radiation with the measured cross polar level below 15 dB along the broadside direction.

Fig. 9 depicts the peak gain variation of the proposed MIMO DRA. It is noted that for *Port1* the simulated and measured gain ranges from 3.85–7.63 dBi and 3.34–7.4 dBi, respectively. The simulated and measured peak gain for *Port2* varies from 2.56–8.07 dBi and 2.34–7.9 dBi, respectively. The antenna element 'DRA-2' behaves in the similar fashion and therefore, the radiation pattern is not shown for brevity.

## 4 MIMO performance evaluation

To evaluate the MIMO/diversity performance of the proposed antenna various key parameters i.e. ECC, diversity gain, CCL and TARC are studied in the subsequent sections.

### *4.1 Envelope correlation coefficient*

ECC is one of the prime performance metric of multi antenna systems and it describes how the communication channels are isolated or correlated with each other. This takes into account the radiation pattern of the antenna and delineate how much the radiation pattern in multi antenna systems affect each other. Under the certain propagation conditions, ECC between the *i*th and *j*th antenna elements can be computed from complex correlation coefficient $\rho_{cij}$ as [4, 13], (see (1)) where Ω refers to solid angle, $E_\theta = E_\theta(\Omega)$ and $E_\phi = E_\phi(\Omega)$ are the $\theta$ and $\phi$ polarised active electric field patterns of the antennas. XPR is the cross polarisation power ratio of the incident waves, $P_\theta = P_\theta(\Omega)$ and $P_\phi = P_\phi(\Omega)$ are the $\theta$ and $\phi$ components of the angular density function of the incoming waves, $G_\theta$ and $G_\phi$ are the $\theta$ and $\phi$ components of the realised active power gain patterns of the antennas. Assuming

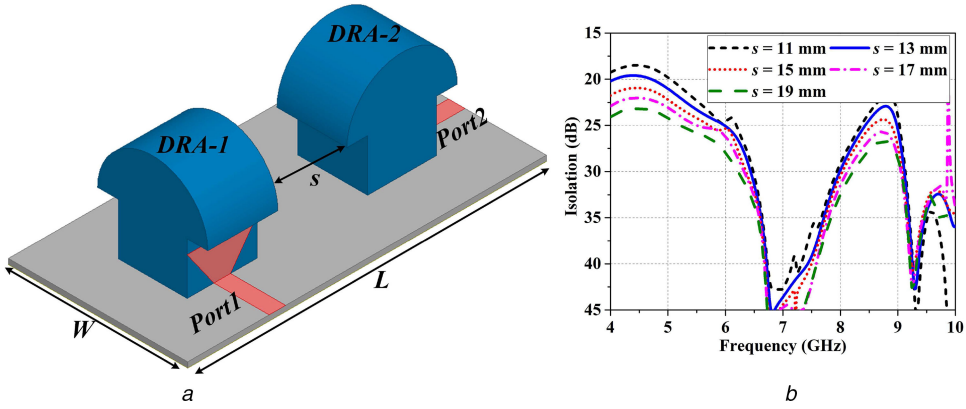


**Fig. 6** *Schematic of the dual element MIMO DRA and its isolation performance for different values inter element spacing s*
***(a)*** Schematic of the proposed MIMO DRA ($L = 52$ mm, $W = 26$ mm, $s = 13$ mm), ***(b)*** Simulated isolation of proposed MIMO DRA for different values of inter element spacing $s$

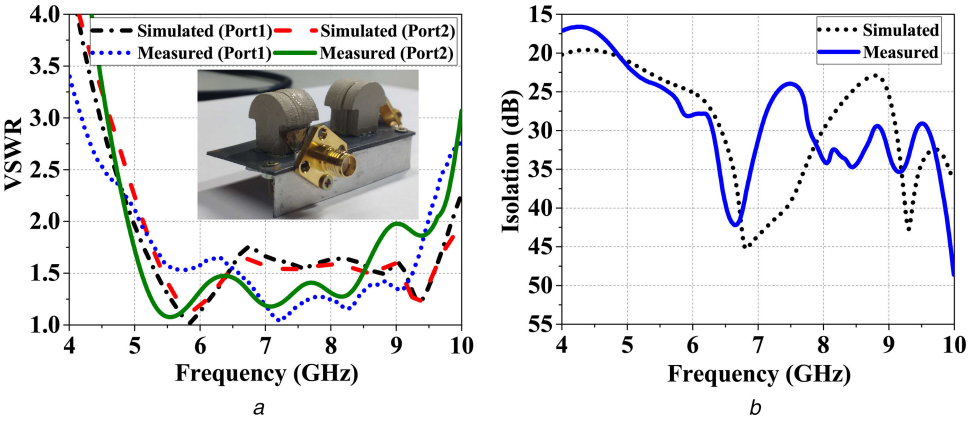


**Fig. 7** *Simulated and measured response of the proposed dual element MIMO DRA*
***(a)*** VSWR, ***(b)*** Isolation

isotropic/uniform propagation scenario [4], we have XPR = 1, $P_\theta(\theta) = P_\phi(\theta) = (1/4\pi)$ and $P_\theta(\phi) = P_\phi(\phi) = 1$ and using $G_{\theta i/j} = E_{\theta i/j} \cdot E^*_{\theta i/j}$ and $G_{\phi i/j} = E_{\phi i/j} \cdot E^*_{\phi i/j}$, (1) can be re-written as

$$\rho_{eij} = \left| \frac{\iint E_{\theta i} \cdot E^*_{\theta j} + E_{\phi i} \cdot E^*_{\phi j} \mathrm{d}\Omega}{\sqrt{\iint E_{\theta i} \cdot E^*_{\theta i} + E_{\phi i} \cdot E^*_{\phi i} \mathrm{d}\Omega \iint E_{\theta j} \cdot E^*_{\theta j} + E_{\phi j} \cdot E^*_{\phi j} \mathrm{d}\Omega}} \right|^2 \quad (2)$$

Both numerically and experimentally, the computation of ECC through radiation pattern of the antenna element is very cumbersome procedure. However, an alternate way to calculate ECC is to use S-Parameters, assuming the antenna elements are lossless and well matched. This method only accounts the isolation between the ports of the antennas and does not consider the mutual coupling between radiated fields. For the two element antenna system, the ECC can be expressed as [3, 31]:

$$\rho_{e12} = \frac{|S^*_{11}S_{12} + S^*_{21}S_{22}|^2}{(1 - (|S_{11}|^2 + |S_{21}|^2))(1 - (|S_{22}|^2 + |S_{12}|^2))} \quad (3)$$

Fig. 10*a* depicts the simulated and measured ECC between two antenna elements using the S-Parameters. Moreover, the magnitude and phase of $E_\theta$ and $E_\phi$ are extracted from Ansoft HFSS to calculate ECC using (2) and the results are depicted in Fig. 10*a* as well as tabulated in Table 1. It is observed that across the entire operating band the ECC < 0.01, satisfying the low-EC criteria (ECC < 0.3 [3]) for MIMO system.

The diversity gain $G_\mathrm{d}$ can be calculated according to following equation [21]:

$$G_\mathrm{d} = 10e_p \quad \text{where} \quad e_p = \sqrt{1 - |0.99\rho_e|^2} \quad (4)$$

Using (4), the measured diversity gain is nearly 10 dB over the entire bandwidth.

### 4.2 Channel capacity loss

Theoretically, the capacity provided by an uncorrelated Rayleigh fading MIMO channels increases linearly with the number of antennas. However, the correlated environment will induce a loss in the channel capacity. Assuming only the receiving antennas are correlated and for high signal to noise ratio (SNR), the loss induced in the capacity for $2 \times 2$ MIMO systems can be evaluated using the following equations [8, 10]:

$$C_\mathrm{loss} = -\log_2 \det(\boldsymbol{\psi}^\mathrm{R}) \quad (5)$$

where $\boldsymbol{\psi}^\mathrm{R}$ is the receiving antenna correlation matrix and is defines as,

$$\boldsymbol{\psi}^\mathrm{R} = \begin{pmatrix} \rho_{11} & \rho_{12} \\ \rho_{21} & \rho_{22} \end{pmatrix} \quad (6)$$

where the matrix elements are defined as:

$$\rho_{ii} = 1 - (|S_{ii}|^2 + |S_{ij}|^2) \text{ and } \rho_{ij} = -(S^*_{ii}S_{ij} + S^*_{ji}S_{jj}) \text{ for } i, j = 1 \text{ or } 2. \quad (7)$$

The simulated and measured variation of CCL (bps/Hz) with frequency is shown in Fig. 10*b*. It is found that $C_\mathrm{loss}$ is under 0.5 bps/Hz throughout the operating bandwidth. For a $2 \times 2$ uncorrelated MIMO systems, the channel capacity for SNR = 20 dB is 11.2 bps/Hz [32]. Therefore, a loss of 0.5 bps/Hz in the channel capacity can be acceptable for practical MIMO systems.

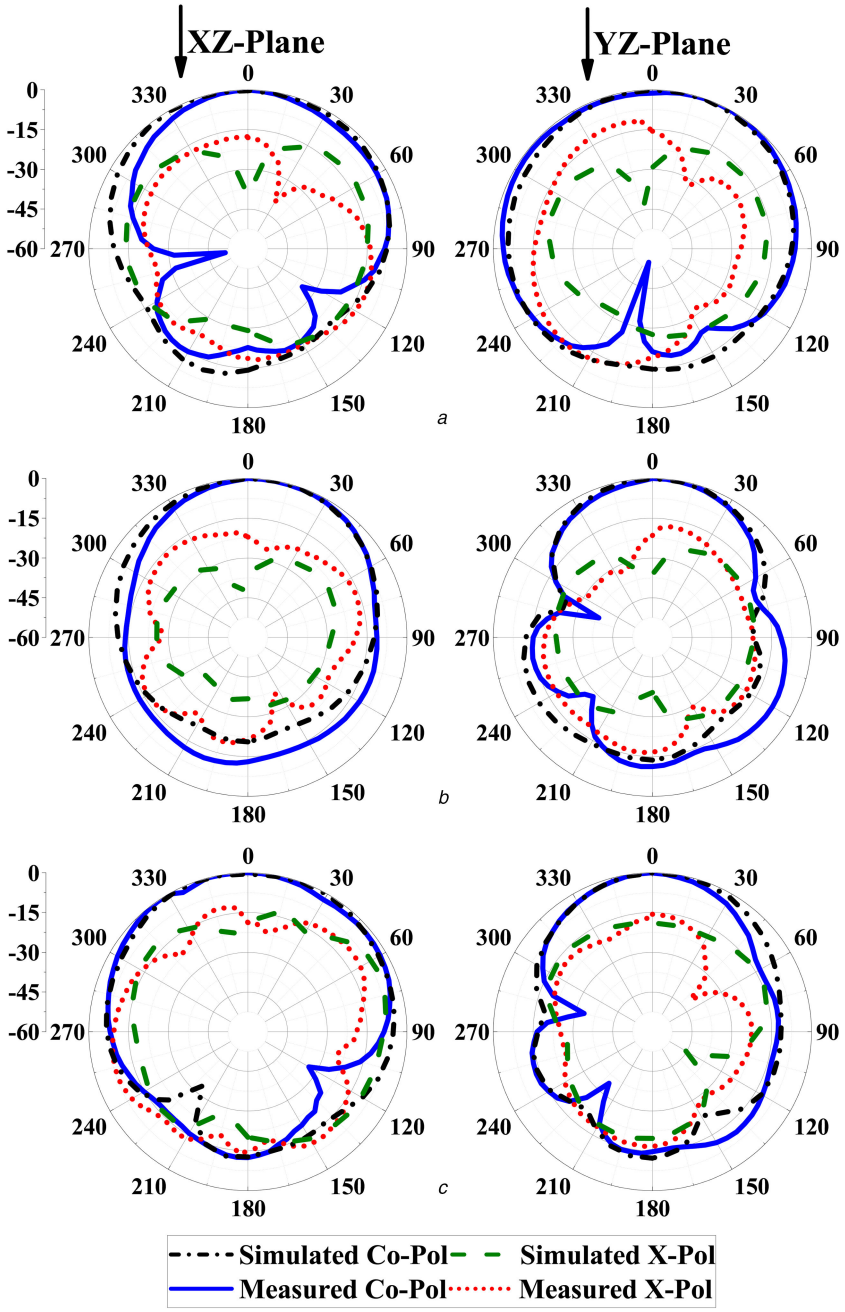


**Fig. 8** *Normalised radiation pattern of the proposed antenna for DRA-1 with other port terminated with matched load at the following frequencies* ***(a)*** 5.5 GHz, ***(b)*** 7 GHz, ***(c)*** 9 GHz

### *4.3 Total active reflection coefficient*

For better characterisation of bandwidth and radiation performance of MIMO system, the TARC is considered. TARC for multi-port antenna system is defined as the ratio of square root of total reflected power to the square root of total incident power [3],

$$\Gamma_a^t = \frac{\sqrt{\sum_{i=1}^{N} |b_i|^2}}{\sqrt{\sum_{i=1}^{N} |a_i|^2}} \tag{8}$$

where $N$ is total number of antenna elements, $a_i$ is the incident signal and $b_i$ is the reflected signal. In terms of S-Parameters, TARC for a two-port MIMO system is defined as [3, 9]:

$$\Gamma_a^t = \frac{\sqrt{(|S_{11} + S_{12}e^{j\theta}|^2) + (|S_{21} + S_{22}e^{j\theta}|^2)}}{\sqrt{2}} \tag{9}$$

where $\theta$ is the input feeding phase and $S_{ij}$ are the associated S-Parameters of the antenna. TARC considers both the mutual coupling and random-signal combinations between ports. Based on TARC, VSWR for MIMO system can be defined as [10]:

$$\text{VSWR}_{\text{MIMO}} = \frac{1 + \Gamma_a^t}{1 - \Gamma_a^t} \tag{10}$$

Fig. 11 presents the calculated $\text{VSWR}_{\text{MIMO}}$ for a set of seven excitation phase ranging from 0° to 180°.

It is observed that VSWR curves retain the original behaviour of a single antenna characteristics. However, the bandwidth is changed because $\text{VSWR}_{\text{MIMO}}$ takes into account the mutual coupling and phase of incident wave.

### *4.4 MIMO antenna efficiency*

The total efficiency of the antenna for *Port1* and *Port2* is expressed as [4, 21]:

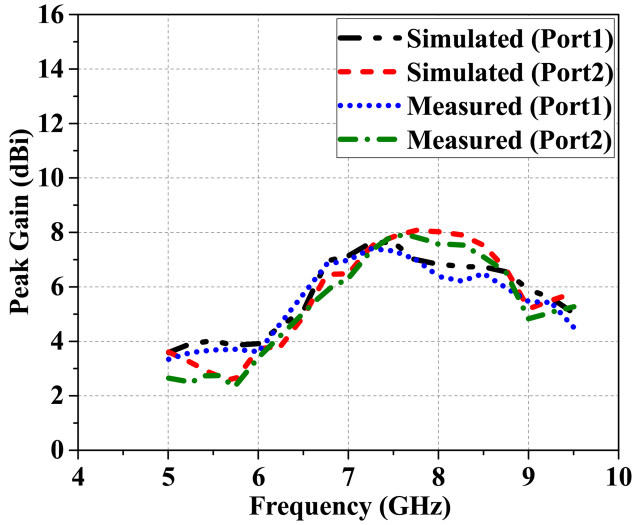


**Fig. 9** *Simulated and measured peak gain variation of proposed MIMO DRA*

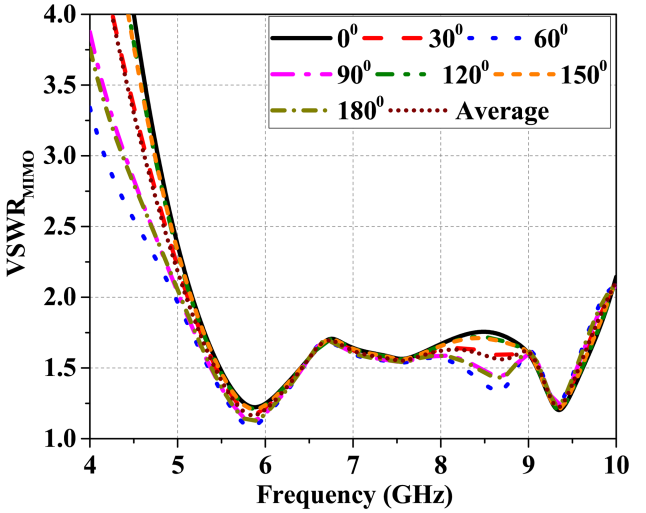


**Fig. 11** *Calculated $VSWR_{MIMO}$ of proposed MIMO-DRA for a set of seven excitation phase*

$$\rho_{eij} \simeq |\rho_{cij}|^2 = \left| \frac{\iint \mathrm{XPR} \cdot E_{\theta i} \cdot E^*_{\theta j} \cdot P_\theta + E_{\phi i} \cdot E^*_{\phi j} \cdot P_\phi \mathrm{d}\Omega}{\sqrt{\iint \mathrm{XPR} \cdot G_{\theta i} \cdot P_\theta + G_{\phi i} \cdot P_\phi d\Omega \iint \mathrm{XPR} \cdot G_{\theta j} \cdot P_\theta + G_{\phi j} \cdot P_\phi \mathrm{d}\Omega}} \right|^2 \quad (1)$$

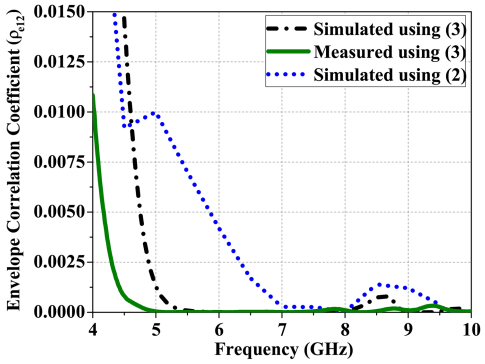


*a*

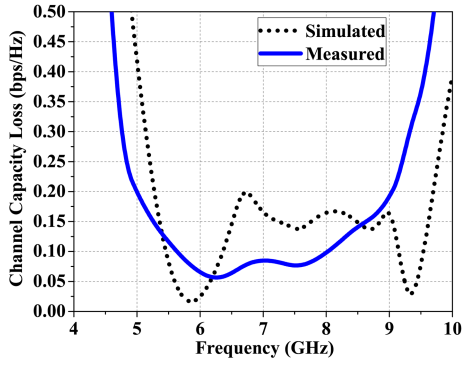


*b*

**Fig. 10** *Simulated and measured*
***(a)*** Envelope correlation coefficient, ***(b)*** Channel capacity loss

**Table 1** ECC values calculated using (2)

| Freq., GHz | 4 | 4.5 | 5 | 5.5 | 6 | 6.5 |
|---|---|---|---|---|---|---|
| ECC | 0.0276 | 0.0092 | 0.01 | 0.007 | 0.0042 | 0.0017 |
| freq., GHz | 7 | 7.5 | 8 | 8.5 | 9 | 9.5 |
| ECC | $2.74 \times 10^{-4}$ | $2.68 \times 10^{-5}$ | $2.75 \times 10^{-5}$ | 0.0014 | 0.0012 | $3.88 \times 10^{-4}$ |

$$\eta_{1t} = \eta_{1,\mathrm{rad}}(1 - |S_{11}|^2 - |S_{12}|^2) \quad (11)$$

$$\eta_{2t} = \eta_{2,\mathrm{rad}}(1 - |S_{22}|^2 - |S_{21}|^2) \quad (12)$$

The simulated efficiency calculated using (11) and (12) is greater than 80% throughout the operating band.

## 5 Conclusion

A dual element wideband MIMO DRA has been presented. A mushroom shaped DRA having wideband characteristics has been utilised to implement two element MIMO DRA which offers polarisation diversity. The proposed antenna offers an impedance bandwidth of 61% (5.08–9.5 GHz) for *Port1* and 65% (4.89–9.61 GHz) for *Port2*. Over the operating bandwidth, the measured input port isolation is better than 20 dB. The proposed antenna is radiating efficiently and exhibits broadside radiation with the cross polar level below 15 dB. The peak gain for *Port1* ranges from 3.34 to 7.40 dBi, whereas for *Port2* it ranges from 2.34 to 7.9 dBi. Apart from conventional antenna parameters, MIMO/diversity performance parameters has also been studied. The ECC is well below 0.01, satisfying the low ECC criteria (ECC < 0.3) for a MIMO system. The diversity gain achieved by the antenna is 10 dB and the capacity loss induced in the channel is below 0.5 bps/Hz over the operating bandwidth. The presented results confirm that an effective MIMO/diversity performance has been achieved. The proposed antenna can be useful for WLAN and upper UWB frequency band applications.

## 6 References


[1] Shannon, C.E.: 'A mathematical theory of communication', *Bell Syst. Tech. J.*, 1948, **27**, pp. 623–656

[2] Allen, B., Malik, W.Q., Smith, P.J., *et al.*: 'Demystifying MIMO', *IET Commun. Eng.*, 2006, **4**, (6), pp. 38–42

[3] Sharawi, M.S.: 'Printed multi-band MIMO antenna systems and their performance metrics', *IEEE Antennas Propag. Mag.*, 2013, **55**, (5), pp. 218–232

[4] Karaboikis, M.P., Papamichael, V.C., Tsachtsiris, G.F., *et al.*: 'Integrating compact printed antennas onto small diversity/MIMO terminals', *IEEE Trans. Antennas Propag.*, 2008, **56**, (7), pp. 2067–2078

[5] Konanur, A.S., Gosalia, K., Krishnamurthy, S.H., *et al.*: 'Increasing wireless channel capacity through MIMO systems employing co-located antennas', *IEEE Trans. Microw. Theory Tech.*, 2005, **53**, (6), pp. 1837–1844

[6] Chae, S.H., Oh, S.K., Park, A.O.: 'Analysis of mutual coupling, correlations, and TARC in WiBro MIMO array antenna', *IEEE Antennas Wirel. Propoag.Lett.*, 2007, **6**, pp. 122–125

[7] Zhou, X., Quan, X., Li, R.: 'A dual-broadband MIMO antenna system for GSM/UMTS/LTE and WLAN handsets', *IEEE Antennas Wirel. Propag. Lett.*, 2012, **11**, pp. 551–554
[8] See, C.H., Abd-Alhameed, R.A., Abidin, Z.Z., *et al.*: 'Wideband printed MIMO/diversity monopole antenna for WiFi/WiMax applications', *IEEE Trans. Antennas Propag.*, 2012, **60**, (4), pp. 2028–2035
[9] Su, S.W., Lee, C.T., Chang, F.S.: 'Printed MIMO-antenna system using neutralization-line technique for wireless USB-dongle applications', *IEEE Trans. Antennas Propag.*, 2012, **60**, (2), pp. 456–463
[10] Valderas, D., Crespo, P., Ling, C.: 'UWB portable printed monopole array design for MIMO communications', *Microw. Opt. Technol. Lett.*, 2010, **52**, (4), pp. 889–895
[11] Liu, L., Cheung, S.W., Yuk, T.I.: 'Compact MIMO antenna for portable devices in UWB applications', *IEEE Trans. Antennas Propag.*, 2013, **61**, (8), pp. 4257–4264
[12] Toktas, A., Akdagli, A.: 'Compact multiple-input-multiple-output antenna with low correlation for ultra-wideband applications', *IET Microw. Antennas Propag.*, 2015, **9**, (8), pp. 822–829
[13] Sarkar, D., Singh, A., Saurav, K., *et al.*: 'Four-element quad-band multiple-input-multiple-output antenna employing split-ring resonator and inter-digital capacitor', *IET Microw. Antennas Propag.*, 2015, **9**, (13), pp. 1453–1460
[14] Lee, H., Lee, B.: 'Compact broadband dual-polarized antenna for indoor MIMO wireless communication systems', *IEEE Trans. Antennas Propag.*, 2016, **64**, (2), pp. 766–770
[15] Mongia, R.K., Bhartia, P.: 'Dielectric resonator antennas-A review and general design relations for resonant frequency and bandwidth', *Int. J. RF Microw. Comput.-Aided Eng.*, 1994, **4**, (3), pp. 230–247
[16] Ishimiya, K., Langbacka, J., Ying, Z., *et al.*: 'A compact MIMI DRA antenna'. Proc. IEEE Int. Workshop on Antenna Technology: Small Antennas and Novel Metamaterials (iWAT '08), Chiba, Japan, March 2008, pp. 286–289
[17] Ishimiya, K., Ying, Z., Langbacka, J.: 'A compact MIMO DRA for 802.11n application'. IEEE Antennas and Propagation Society Int. Symp., San Diego, CA, July 2008
[18] Yan, J.B., Bernhard, J.T.: 'Design of a MIMO dielectric resonator antenna for LTE femtocell base stations', *IEEE Trans. Antennas Propag.*, 2012, **60**, (2), pp. 438–444
[19] Thamae, L.Z., Wu, Z.: 'Dielectric resonator based multiple-input-multiple-output antennas and channel characteristic analysis', *IET Microw. Antennas Propag.*, 2012, **6**, (9), pp. 1084–1089
[20] Yan, J.B., Bernhard, J.T.: 'Implementation of a frequency agile MIMO dielectric resonator antenna', *IEEE Trans. Antennas Propag.*, 2013, **61**, (7), pp. 3434–3441
[21] Roslan, S.F., Kamarudin, M.R., Khalily, M., *et al.*: 'An MIMO rectangular dielectric resonator antenna for 4G applications', *IEEE Antennas Wirel. Propag. Lett.*, 2014, **13**, pp. 321–324
[22] Johnstone, J.C., Podilchak, S.K., Clénet, M., *et al.*: 'A compact cylindrical dielectric resonator antenna for MIMO applications'. 2014 IEEE Antennas and Propagation Society Int. Symp. (APSURSI), Memphis, TN, 2014, pp. 1938–1939
[23] Sharawi, M.S., Podilchack, S.K., Antar, Y.M.M.: 'A low profile dual-band DRA-based MIMO antenna system for wireless access points'. 2015 IEEE Int. Symp. on Antennas and Propagation and USNC/URSI National Radio Science Meeting, Vancouver, BC, 2015, pp. 707–708
[24] Hussai, M.T., Hammi, O., Sharawi, M.S., *et al.*: 'A dielectric resonator based millimeter-wave MIMO antenna array for hand-held devices'. 2015 IEEE Int. Symp. on Antennas and Propagation and USNC/URSI National Radio Science Meeting, Vancouver, BC, 2015, pp. 3–4
[25] Hussai, M.T., Sharawi, M.S., Podilchack, S.K., *et al.*: 'Closely packed millimeter-wave MIMO antenna arrays with dielectric resonator elements'. 2016 10th European Conf. on Antennas and Propagation (EuCAP), Davos, 2016, pp. 1–4
[26] Roslan, S.F., Kamarudin, M.R., Khalily, M., *et al.*: 'An MIMO F-shaped dielectric resonator antenna for 4G applications', *Microw. Opt. Technol. Lett.*, 2015, **57**, (12), pp. 2931–2936
[27] Nasir, J., Jamaluddin, M.H., Khalily, M., *et al.*: 'Design of an MIMO dielectric resonator antenna for 4G aplications', *Wirel. Pers. Commun.*, 2016, **88**, pp. 525–536
[28] Liang, X.L., Denidni, T.A.: 'H-shaped dielectric resonator antenna for wideband applications', *IEEE Antennas Wirel. Propag. Lett.*, 2008, **7**, pp. 163–166
[29] Liang, X.L., Denidni, T.A., Zhang, L.N.: 'Wideband L-shaped dielectric resonator antenna with conformal inverted-trapezoidal patch feed', *IEEE Trans. Antennas Propag.*, 2009, **57**, (1), pp. 271–274
[30] Rashidian, A., Shafai, L., Klymyshyn, D.M.: 'Compact wideband multimode dielectric resonator antennas fed with parallel standing strips', *IEEE Trans. Antennas Propag.*, 2012, **60**, (11), pp. 5021–5031
[31] Blanch, S., Romeu, J., Corbella, I.: 'Exact representation of antenna system diversity performance from input parameter description', *Electron. Lett.*, 2003, **39**, (9), pp. 705–706
[32] Karimkashi, S., Kishk, A.A., Kajfez, D.: 'Antenna array optimization using dipole models for MIMO applications', *IEEE Trans. Antennas Propag.*, 2011, **59**, (8), pp. 3112–3116